Shape from Single Scattering
for Translucent Objects

Chika Inoshita[1], Yasuhiro Mukaigawa[1], Yasuyuki Matsushita[2], Yasushi Yagi[1]

[1]Osaka University   [2]Microsoft Research Asia

Abstract. Translucent objects strongly scatter incident light. Scattering makes the problem of estimating shape of translucent objects difficult, because reflective or transmitted light cannot be reliably extracted from the scattering. In this paper, we propose a new shape estimation method by directly utilizing scattering measurements. Although volumetric scattering is a complex phenomenon, single scattering can be relatively easily modeled because it is a simple one-bounce collision of light to a particle in a medium. Based on this observation, our method determines the shape of objects from the observed intensities of the single scattering and its attenuation. We develop a solution method that simultaneously determines scattering parameters and the shape based on energy minimization. We demonstrate the effectiveness of the proposed approach by extensive experiments using synthetic and real data.

1 Introduction

In real-world scenes, there are many translucent objects around us, such as wax, plastic products, and precious stones. Inside a translucent object, incident light scatters and randomly travels. Although vision-based shape estimation techniques are maturing, it is still difficult to estimate the shape of translucent objects. Passive approaches based on triangulation require a target objects to be well-textured, and active methods tend to fail due to strong scattering of the incident light. As pointed out by Godin *et al.* [1], the incident light shows the brightest observation off the object surface for translucent materials due to scattering. Methods based on refractive or transmitted light cannot be directly applied to translucent media where strong scattering exists. Figure 1 shows an example of a failure mode for measuring translucent objects using a commercial 3D laser scanner, Konica-Minolta Vivid 9i. While it works well for human skin, the shape of translucent objects is not accurately estimated due to strong scattering. Shape estimation of translucent objects is still a wide open problem.

While scattering is well studied in computer graphics, it is less discussed in computer vision because the complexity of light interactions renders inverse problems intractable. Therefore, for vision applications, scattering has been regarded as a nuisance and eliminated by various approaches, *e.g.*, polarization [2], coating with diffuse powder [3], and phase-shift measurements [4]. In contrast to these approaches, we propose a new shape estimation method based on the
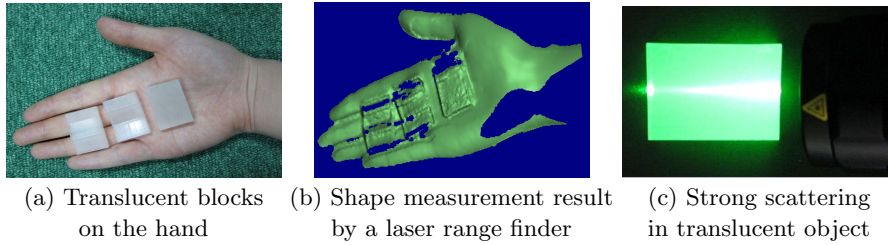
(a) Translucent blocks   (b) Shape measurement result   (c) Strong scattering
    on the hand   by a laser range finder   in translucent object

Fig. 1. Failure mode of shape measurement of translucent objects using a 3D laser scanner.

observed scattering itself. In particular, we develop a method that uses the observation of single scattering, which occurs via a one-bounce collision of light to a particle, and its attenuation along the light path. We derive a solution method from a scattering model that takes into account the refraction, an extinction coefficient, and a phase function.

The primary contributions of our work are as follows. We propose a new shape estimation technique for translucent objects. It introduces the use of scattering as a beneficial signal for determining shape. The proposed method is effective when the target object shows strong scattering where other shape estimation approaches cannot be applied. In fact, since there exist various objects in our daily life that exhibit strong scattering, our method has wide applicability. This work is the first attempt to directly use the observed intensities of single scattering for shape measurement. In addition, we develop an effective solution method based on energy minimization for simultaneously estimating shape and scattering parameters.

2   Related work

Shape-from-intensity is a generic framework for shape measurement based on observed intensities. Various optical phenomena, such as diffuse [5, 6] or specular reflection [7, 8], have been used as cues for shape estimation. Liao *et al.* [9] estimate object's shape from light attenuation, which is inversely proportional to the square of distance. Our method is related to Liao *et al.*'s method because we also use the attenuation of the light although the setting is different.

Refractive lights have been used to measure the shape of transparent objects, because most incident lights to the surface are transmitted inside. Miyazaki and Ikeuchi [10] estimate the object surface by analyzing multiple interreflections in the object by a polarization ray-tracing method. Huynh *et al.* [11] use multi-spectral polarization for obtaining surface normals. Kutulakos and Steger's method [12] performs triangulation from the analyzed transmitted light path. Wetzstein *et al.* [13] use a light field probe to analyze the transmitted light path. Trifonov *et al.*'s method [14] immerses target objects in fluid whose

refractive index is the same as the target and applies tomography for obtaining shape. Hullin *et al.* [15] use a scan-line illumination for transparent objects immersed in fluorescent fluid. While these methods use refracted light, Morris and Kutulakos [16] propose scatter-trace photography focusing on the transparent object that reflects some of the incident light. While these methods are effective, it is not straightforward to apply them to translucent objects due to strong scattering.

Shape measurement methods for objects in scattering media have been also proposed. Narasimhan *et al.* [17] measure the shape of target objects in scattering media by light stripe scanning and photometric stereo. Kim *et al.* [18] remove scattering light by angular filtering and estimate the shape by tomography. Treibitz and Schechner [19] not only remove backscattering in an underwater scene, but also estimate the scene depth based on backscattering falloff. Florescu *et al.* [20] apply the optical tomography using observed single scattering based on a radiative transfer equation and reconstruct the attenuation parameter of the 3D volume. While these are related, these cannot be directly applied to estimate the shape of translucent objects. More recently, characteristics of scattering media have been actively studied. Mukaigawa *et al.* [21] propose a method for separating single and multiple scatterings and analyze the light transport. Narasimhan *et al.* [22] dilute scattering media to reduce multiple scattering for estimating scattering parameters. The spatial distribution of scattering media, such as smoke or milk drops, has also been studied [23, 24]. We develop our method based on these studies on the characteristics of scattering.

Scattering has similar properties to interreflections. In fact, scattering can be regarded as interreflections of light in a medium. In the study of shape estimation with the existence of interreflections, there are three major approaches:

1. Elimination of the interreflections: Nayar *et al.* [25] show a method to remove interreflections using high frequency illumination. After the elimination of interreflections, a classic technique, such as Lambertian photometric stereo, can be well applied.
2. Modeling of interreflections: Nayar *et al.* [26] iteratively estimate the shape of concave surface by explicitly modeling the interreflection based on radiosity.
3. Use of the interreflection itself: Liu *et al.* [27] show that the light transport of the interreflections can be used as a cue for shape estimation.

Thus, similar approaches may be applicable for shape measurement of a translucent object. Our approach is close to the third approach where we wish to recover shape from scattering itself.

3   Shape from Single Scattering

3.1   Background

When light travels through a translucent medium, the light scatters in the medium due to collisions with particles. Single scattering is a type of scattering,
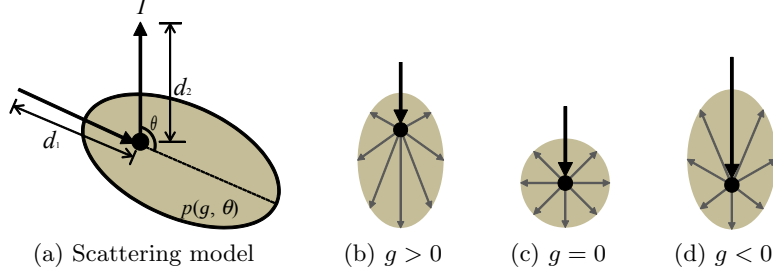
(a) Scattering model   (b) $g > 0$ (c) $g = 0$ (d) $g < 0$

Fig. 2. Illustration of the scattering model and examples of distribution profiles with a varying phase function.

in which light scatters at only once in the medium before reaching a viewer. Figure 2(a) shows a parametric scattering model. In scattering media, the incident light exponentially attenuates with the length of light path by the Lambert-Beer law [28]. It also scatters in the media, and a Henyey-Greenstein phase function [29] is known as a good approximation for the phenomenon. With this phase function, the observed intensity I of single scattering is described as [21, 22]

$$I = sp(g, \theta)e^{-\sigma_t(d_1 + d_2)}, \tag{1}$$

$$p(g, \theta) = \frac{1}{4\pi} \frac{1 - g^2}{(1 + g^2 - 2g\cos\theta)^{\frac{3}{2}}}, \tag{2}$$

where s is a scaling constant that includes the intensity of the incident light and scattering coefficient, σ_t is an extinction coefficient, $(d_1 + d_2)$ represents the length of the light path in the medium, and $p(g, \theta)$ is the phase function. The phase function represents the scattering distribution, and the distribution profile is controlled by a parameter g $(-1 \leq g \leq 1)$. Figures 2(b), (c), and (d) show examples of the distribution profiles produced by varying g.

3.2   Formulation

We formulate the relationship between observed intensities of single scattering and the shape of translucent target. Figure 3 shows our setting for the shape measurement. A translucent object is illuminated from one side and observed from the top. We assume a homogeneous material as a target object and orthographic projection for both illumination and observation. In addition, we ignore multiple scattering for now, but a method for handling it will be explained in later sections.

Figure 4 illustrates a light path of single scattering in a medium. The incident ray $\mathbf{i}_x$ scatters at scattering point (x', y'), and reaches to surface point (x, y). $\mathbf{n}(x, y)$ represents the surface normal and $\mathbf{i}_x = [1, 0, 0]^T$ and $\mathbf{i}_z = [0, 0, 1]^T$ are incident and exitant light vectors, respectively. $\mathbf{r}(x, y)$ is a unit scattering vector
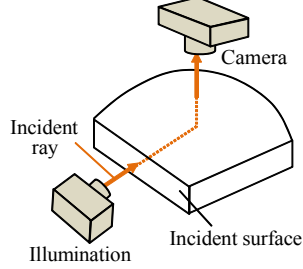
Fig. 3. Setting for shape estimation. A translucent object is illuminated from the side and observed from the top.
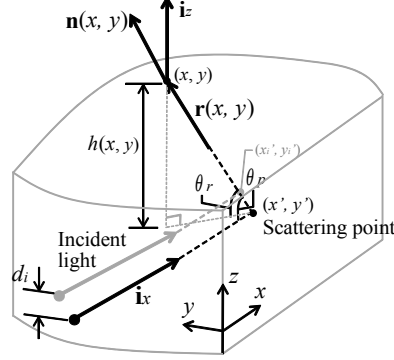
Fig. 4. Light path in the target object. The incident plane is almost planer, and incident light is assumed parallel to x-axis. The illuminated ray reaches to surface point (x, y) changing the travel direction at the scattering point (x', y').

pointing from the scattering point (x', y') to the surface point (x, y). The angle between the incident vector $\mathbf{i}_x$ and the scattering vector $\mathbf{r}(x, y)$ is denoted as θ_p. θ_r represents the projected angle of θ_p on the plane spanned by $\mathbf{r}(x, y)$ and $\mathbf{i}_z$. Our purpose is to estimate the height of the translucent object $h(x, y)$ from the observed intensities $I(x, y)$ at the surface point (x, y) on the surface, where the height of the incident ray is $z = 0$. Scattered incident ray $\mathbf{i}_x$ is finally refracted at the object surface. The angle of refraction obeys Snell's law represented as

$$\mathbf{n}(x, y) \times \mathbf{i}_z = \eta \mathbf{n}(x, y) \times \mathbf{r}(x, y), \tag{3}$$

where η is a refractive index, $\times$ represents a cross-product operator. The total length of the light path becomes the sum of x', which corresponds to the distance from the incident point to scattering point and the distance from the scattering point to the surface point, $h(x, y)/\sin \theta_r$. Since the intensity of single scattering is modeled as Eq. (1), the observed intensity is represented by

$$I(x, y) = s F_t^{in} F_t^{out}(x, y) p(g, \theta_p) e^{-\sigma_t \left(x' + \frac{h(x, y)}{\sin \theta_r} \right)}, \tag{4}$$

where s is a scaling constant, $F_t^{out}(x, y)$ represents the Fresnel transmittance on the surface point (x, y), and F_t^{in} is the constant Fresnel transmittance on the incident point because the incident light is perpendicular to the incident plane. Equation (4) shows that the observed intensity depends on both the geometric shape and scattering parameters including extinction parameter σ_t, refractive index η, and phase function parameter g. Given these scattering parameters, the height of the translucent object is determined up to an unknown offset due to s

by

$$h(x,y) = \frac{\sin \theta_r}{\sigma_t} \left(\log s + \log F_t^{in} + \log F_t^{out}(x,y) + \log p(g, \theta_p) - \log I(x,y) \right)$$
$$-x' \sin \theta_r. \quad (5)$$

4   Solution method

In the previous section, we described a basic theory of the shape from single scattering. However, in reality, we cannot directly estimate the object height $h(x,y)$ by Eq. (5) due to the unknown parameters. In addition, the observed intensities include the contributions not only from single scattering but also from multiple scattering. In this section, we discuss a solution method for these problems. In our method, we assume that the refractive index η is known because it can be directly measured using a refractometer.

In our method, we employ an energy minimization approach for simultaneously determining both the shape and scattering parameters. When the unknown parameters and height are correctly estimated, Eq. (4) should produce the intensity that becomes equivalent to the observed intensity $I(x,y)$. Although we can estimate the unknown parameters by seeking parameters, which generate the observed intensity, parameter estimation tends to be unstable due to a larger number of unknowns than the captured intensity. To reliably derive a solution to this problem, we use multiple $n(2 \leq n)$ images that are captured by changing the height of the incident ray. Namely, we record multiple intensities $I_i(x,y)$ with varying heights of the incident rays $z = d_i$ $(i = 1, \ldots, n)$ as shown in Fig. 4. Now we have n intensity observations per scene point $I_i(x,y)$ as

$$I_i(x,y) = s F_t^{in} F_t^{out}(x,y) p(g, \theta_p) e^{-\sigma_t (x'_i + \frac{h(x,y) - d_i}{\sin \theta_r})}, \quad i = 1, \ldots, n. \quad (6)$$

We also take into account the signal-to-noise ratio of the observed intensities; the darker observations suffer more from image noise while the brighter observations are more reliable. We incorporate this as a weighting factor w_i when determining the unknown parameters. Based on these, we define an energy function for computing heights $h(x,y)$ and scattering parameters s, g, σ_t as

$$E(h(x,y), s, g, \sigma_t) = \sum_i w_i \sum_{x,y} \left(I_i(x,y) - I_i^{gen}(h(x,y), s, g, \sigma_t) \right)^2, \quad (7)$$

where I_i^{gen} is the generated intensity based on Eq. (6), and w_i is a weighting factor for reducing the effect of noise. We define the weighting factor w_i as

$$w_i = \frac{\sum_{x,y} I_i(x,y)}{\sum_{k=1}^{n} \sum_{x,y} I_k(x,y)}. \quad (8)$$

The energy function E evaluates the closeness between observed intensity and generated intensity based on Eq. (6). The minimizer of the energy function E

gives us estimates of the height $h(x, y)$ per-pixel and scattering parameters s, g and σ_t as

$$\{h(x, y), s, g, \sigma_t\} = \underset{h(x,y),s,g,\sigma_t}{\mathrm{argmin}} \; E(h(x, y), s, g, \sigma_t). \tag{9}$$

We describe the optimization method in the following section.

4.1   Implementation

This section describes the implementation details of the solution method. Our method uses a non-linear optimization because of the non-convexity of Eq. (7) with respect to the unknown parameters. We now describe the computation method of the initial guess of the height $h(x, y)$ and the following optimization strategy.

Estimation of initial shape To obtain an initial guess of the estimated parameters, we use the initial shape $h^0(x, y)$ that can be computed by ignoring refraction ($\eta = 1$). When $\eta = 1$, the scattering vector coincides with the output vector $\mathbf{i}_z$, the 2D projection of the scattering point (x', y') becomes identical with the surface point (x, y), and Fresnel transmittance $F_t^{out}(x, y)$ is constant because the refraction is disregarded. Since the angle θ_p equals to $\pi/2$, phase function $p(g, \theta_p)$ becomes constant. Therefore, the intensity generated from initial height $h^0(x, y)$ is described as

$$I_i^0(x, y) = Se^{-\sigma_t(h^0(x,y)+x-d_i)}, \quad S = sF_t^{in}F_t^{out}p\left(g, \frac{\pi}{2}\right). \tag{10}$$

Here, unknown parameters are the height $h^0(x, y)$, scaling constant S, and extinction coefficient σ_t. Using a pair of intensity observations $I_i(x, y)$ and $I_j(x, y)$ taken by different heights of incident rays d_i and d_j, the extinction coefficient is calculated as

$$\sigma_t = \frac{\log I_i(x, y) - \log I_j(x, y)}{d_i - d_j} \quad (d_i \neq d_j). \tag{11}$$

In practice, we take the average as the estimate of σ_t using all the pairs of d_i and d_j. We employ an intensity at the incident point as the initial scaling constant S as the scaling without attenuation. The initial guess of the height $h^0(x, y)$ is therefore described as

$$h^0(x, y) = \frac{1}{\sigma_t} \left(\log S - \log I_i(x, y)\right) - x + d_i, \tag{12}$$

and is estimated using the parameters σ_t and S. We use this initial guess as an input to the optimization: $h(x, y) \leftarrow h^0(x, y)$.

Optimization Now we estimate the shape and parameters by minimizing Eq. (9) using h^0 as the initial guess of the shape. The unknowns to be estimated are per-pixel height $h(x, y)$ and scattering parameters s, g, and σ_t. To efficiently avoid local minima, we use a two-step approach for the optimization. Namely, we first apply the Particle Swarm optimization [30] for limiting the search range in a coarse manner, and then use the Nelder-Mead method [31] for finding the optimal parameter set in a fine scale.

Extraction of single scattering As discussed above, actual observations consist of both single and multiple scatterings as shown in Fig. 1(c). To separate the single scattering component from multiple scattering, we utilize a separation method [21] which uses projector as a light source as shown in Fig. 3. The extracted single scattering component is used as input for our method. Readers are referred to [21] for the details of the separation method.

5   Experiments

We assess the effectiveness of the proposed method using both synthetic and real-world scenes. With the synthetic scenes, we assess the accuracy of the proposed method by comparing with the ground truth. For the real-world scenes, we prepare two objects where the ground truth shape is available while the scattering parameters are unknown.

5.1   Synthetic scenes

For the synthetic scene experiment, we used one 1-D curved surface, one 1-D discontinuous surface, and one 2-D discontinuous surface $h(x)$ as the scenes; Scenes A, B, and C. For each scene, we simulated intensity observations $I_i(x)$ with varying heights of incident rays $d_i = 0.2 \times i$[mm], $i = 0, \cdots, 9$ using the scattering model of Eq. (6). We added Gaussian noise to the intensity observations at 5 levels ($\mu = 0$ and $\sigma = 0, 5, 10, 15, 20$). The optical parameters are consistently set to $\eta = 1.2$, $g = 0.1$, $\sigma_t = 15$, and $s = 50000$.

Figure 5(a) shows Scene A and (b) shows simulated intensity observation in the case of Gaussian noise $\sigma = 10$. From this intensity, we estimate the object shape. Figure 5(c) shows the estimated result of Scene A. The initial height is globally skewed due to the inaccurate assumption of the refractive index $\eta = 1$ and local deformations due to observation noise. Especially, when Gaussian noise levels are $\sigma = 15$ and 20, estimated shapes become noisier as the length of light paths are greater because of the low S/N ratio. However, the optimized results consistently agree well with the ground truth except for some fluctuations. Figure 5(d) shows RMSE of the estimated height at each noise level. Although the RMSE increases according to the noise amplitude, the overall errors are small and show the accuracy of the method. Estimated scattering parameters and the RMSE values are summarized in Table 1. With small noise, the scaling parameter s and extinction coefficient σ_t are almost correct. The scattering parameter g

(a) Synthetic scene

(b) Intensity observations

(c) Estimated result
at each noise level
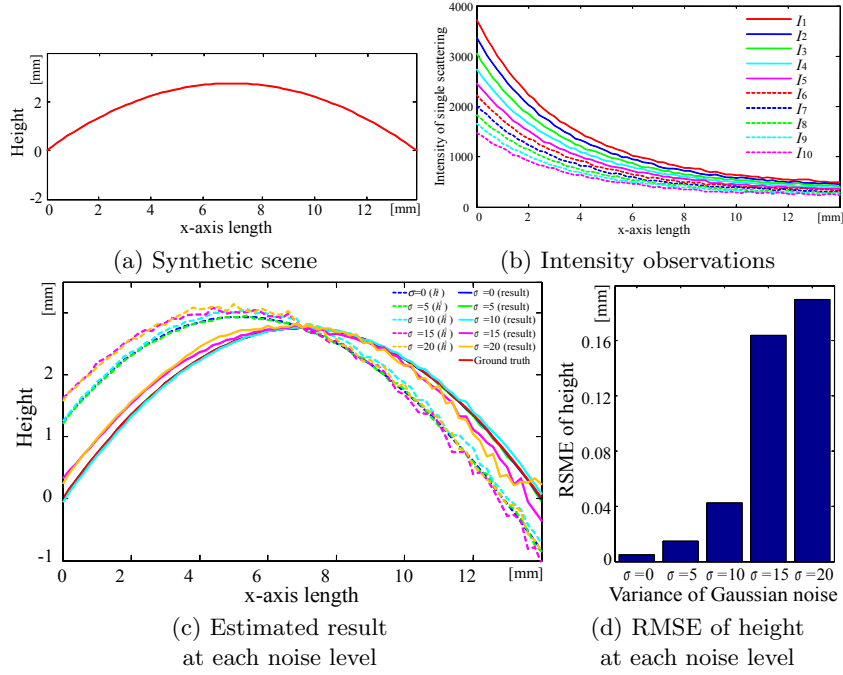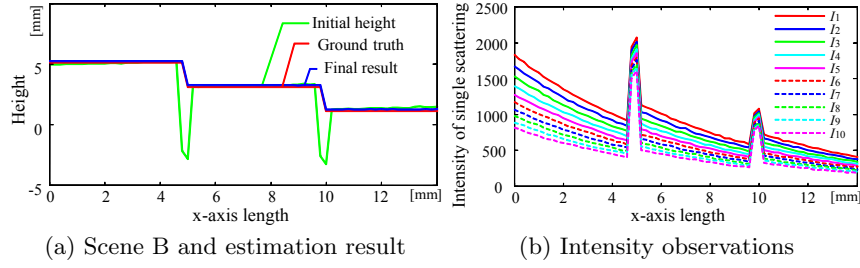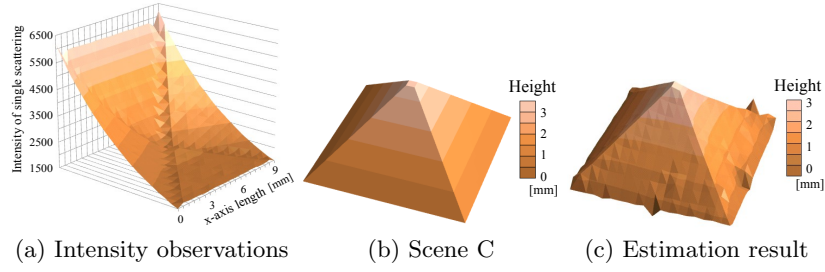
(d) RMSE of height
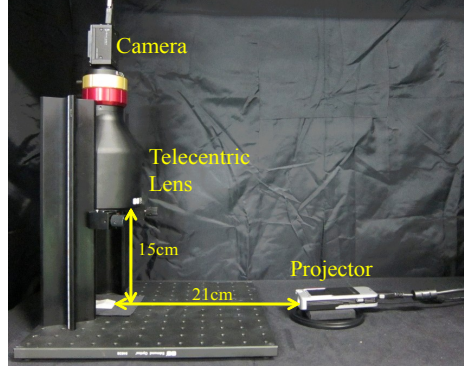at each noise level

Fig. 5. Estimated heights of Scene A

Table 1. Estimated parameters and RMSE of estimated height at each noise level.

	Scaling constant s	Parameter g	Extinction coefficient σ_t [mm^{-1}]	RMSE of height [mm]
Ground truth	5.0×10^4	0.1	1.5	-
$\sigma = 0$	5.08×10^4	0.069	15.0	0.05×10^{-1}
$\sigma = 5$	4.95×10^4	0.007	15.0	0.15×10^{-1}
$\sigma = 10$	4.95×10^4	0.002	15.0	0.42×10^{-1}
$\sigma = 15$	6.09×10^4	-0.002	16.0	1.64×10^{-1}
$\sigma = 20$	6.33×10^4	0.003	16.1	1.90×10^{-1}

has a larger deviation from its ground truth. Although g controls the scattering distribution, it effects to both intensity scale and intensity attenuation depending to object shape. Thus, estimating g becomes more difficult than estimating other parameters.

Other experimental results using synthetic 1-D stepped shape (Scene B) and 2-D pyramid like shape (Scene C). The ground truth and the estimated result in the case of Gaussian noise $\sigma = 10$ are shown in Fig. 6(a) and Fig. 7(b). For these asymmetric and discontinuous scenes as well, the estimation well converges near to the ground truth.

(a) Scene B and estimation result   (b) Intensity observations

Fig. 6. Estimated heights of discontinuous Scene B

(a) Intensity observations   (b) Scene C   (c) Estimation result

Fig. 7. Estimated heights of discontinuous Scene C

Fig. 8. Experimental setting. A projector is placed on the side of the object, and a camera is vertically placed, we used a telecentric lens for orthographic projection.

5.2   Real scenes

We also applied the proposed method to real-world scenes. Figure 8 shows the experimental setting. A 3M MPro110 projector is placed on the side of the target object, and a Point Grey Grasshopper camera which has a linear response sensor is vertically placed to obtain a top view. To avoid the perspective effect of the
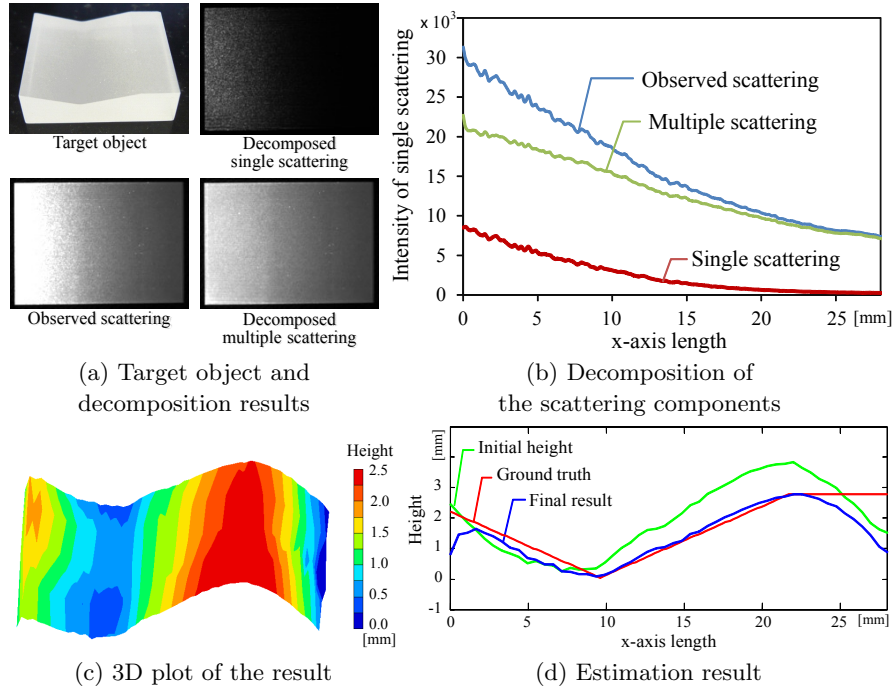
(a) Target object and
decomposition results

(b) Decomposition of
the scattering components

(c) 3D plot of the result

(d) Estimation result

Fig. 9. Experimental result using a concave scene.

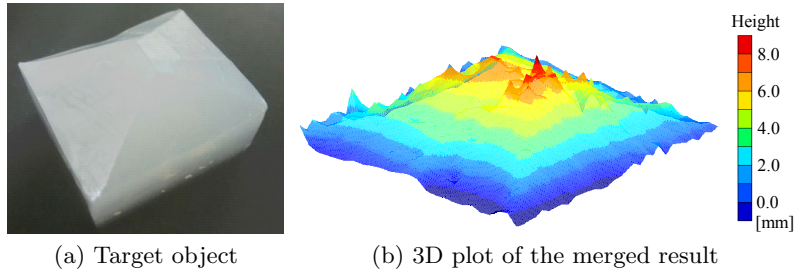

(a) Target object

(b) 3D plot of the merged result

Fig. 10. Experimental results using a asymmetric convex scene. (b) shows the 3D plot
of the merged result.

imaging system, we use an Edmund optics telecentric lens for approximating
an orthographic projection. To perform a comprehensive analysis, we use two
different shapes of translucent objects; one is concave, and the other is convex.
We made concave object using same material as shown in Fig. 1 (b) and convex
object using a colored gelatin. The ground truth of these objects are known for
performing a quantitative evaluation. We set the refractive index η as 1.3. We

captured intensities of single scattering $I_i(x, y)$ ($d_i = 0.25 \times i$[mm], $i = 0, \cdots, 9$) with shifting height of incident light.

Figure 9(a) shows the concave object. The object is illuminated by a projector from its side plane. Figures 9(a) and (b) show the decomposition of the scattering components. The red, green, and blue plots show the intensities of single scattering, multiple scattering, and observed scattering, respectively. It can be seen that single scattering is almost exponentially attenuated with the increased distance from the incident point. Figure 9(c) shows the shape estimation result plotted as a 3D surface. We can see that our method is able to estimate the overall shape of the target except for the flat region. A possible reason for the incorrect estimation is insufficient intensities of single scattering for shape estimation because the light paths are longer for observing this region. In addition, the shape nearby the incident plane did not match the ground truth well due to the bright observation at the incident point and its glare. Estimated scattering parameters are $s = 12118$, $g = 0.042$, and $\sigma_t = 13.244$.

We also show the result of the convex scene in Fig. 10. Figure 10(b) shows the reconstruction result given by single scattering illuminated from front of the target object. Because of insufficient intensities of single scattering, estimated height has large error in back area. To reduce the error, we capture the intensities of single scattering by illuminating from the other side of the target object, and merge the two reconstruction results. Figure 10(c) shows the merged result.

Computation time In this experiment, it takes about 15 minutes to capture images (6 images for extracting single scattering at each of 10 different depths), and it takes about a few hours to compute the shape with an unoptimized Matlab implementation. We compute estimates on Intel Core 2 Duo CPU (3.00 GHz) and 3GB RAM. The size of problem is 74 (71 points for $h(x)$, s, g, and σ_t) in synthetic data, 259 (256 points for $h(x, y)$, s, g, and σ_t) in symmetric real data, and 873 (870 points for $h(x, y)$, s, g, and σ_t) in asymmetric real data.

6   Discussions

In this paper, we proposed a method for estimating the shape of translucent objects based on the attenuation of single scattering. We showed synthetic and real-world results that our method has a potential for accurate modeling of translucent objects, which has been difficult with other appearance-based methods. While the method works well for various translucent objects, the accuracy suffers from low-intensity measurements and high signal-to-noise ratio when optically dense objects are measured, in which multiple scattering dominate the appearance. Another issue of the current approach is its high computational cost. We are interested in looking into more in these aspects for making the approach more practical.

Limitations There are a few limitations in the current method. These limitations will be removed in our future work.

Object shape: Our current formulation requires that the incident plane is planer and incident light in target object is parallel to the x-axis for extracting single scattering using high frequency projection. When projected patterns interfere each other, single scattering cannot be extracted. This assumption needs to be relaxed when it is applied to a more general shape.

Single scattering in an inhomogeneous material: Since our method uses single scattering which exponentially attenuates with constant scattering parameters, we cannot estimate shape of an inhomogeneous material.

Acknowledgment

References

1. Godin, G., Rioux, M., Beraldin, J.A.: An assessment of laser range measurement on marble surfaces. In: Conference on Optical 3D Measurement Techniques. (2001)
2. Chen, T., Lensch, H.P.A., Fuchs, C., Seidel, H.P.: Polarization and phase-shifting for 3d scanning of translucent objects. In: Proc. of IEEE Conference on Computer Vision and Pattern Recognition (CVPR). (2007)
3. Goesele, M., Lensch, H.P.A., Lang, J., Fuchs, C., Seidel, H.P.: Disco - acquisition of translucent objects. In: Proc. ACM SIGGRAPH. (2004) 835–844
4. Gupta, M., Agrawal, A., Veeraraghavan, A., Narasimhan, S.: Structured light 3d scanning in the presence of global illumination. In: Proc. of IEEE Conference on Computer Vision and Pattern Recognition (CVPR). (2011)
5. Horn, B.K.P.: Shape from shading: A method for obtaining the shape of a smooth opaque object from one view. Technical report, Massachusetts Institute of Technology (1970)
6. Woodham, R.J.: Photometric method for determining surface orientation from multiple images. Optical Engineering **19** (1980) 139–144
7. Healey, G., Binford, T.O.: Local shape from specularity. Computer Vision, Graphics, and Image Processing **42** (1987) 62–86
8. Sankaranarayanan, A.C., Veeraraghavan, A., Tuzel, O., Agrawal, A.: Specular surface reconstruction from sparse reflection correspondences. In: Proc. of IEEE Conference on Computer Vision and Pattern Recognition (CVPR). (2010)
9. Liao, M., Wang, L., Yang, R., Gong, M.: Light fall-off stereo. In: Proc. of IEEE Conference on Computer Vision and Pattern Recognition (CVPR). (2007)
10. Miyazaki, D., Ikeuchi, K.: Shape estimation of transparent objects by using inverse polarization raytracing. IEEE Trans. Pattern Analysis and Machine Intelligence (PAMI) **29** (2007) 2018–2030
11. Huynh, C.P., Robles-Kelly, A., Hancock, E.: Shape and refractive index recovery from single-view polarisation images. In: Proc. of IEEE Conference on Computer Vision and Pattern Recognition (CVPR). (2010)

12. Kutulakos, K.N., Steger, E.: A theory of refractive and specular 3d shape by light-path triangulation. In: Proc. of International Conference on Computer Vision (ICCV). (2005)
13. Wetzstein, G., Roodnick, D., Heidrich, W., Raskar, R.: Refractive shape from light field distortion. In: Proc. of International Conference on Computer Vision (ICCV). (2011)
14. Trifonov, B., Bradley, D., .Heidrich, W.: Tomographic reconstruction of transparent objects. In: Proc. of Eurographics Symposium on Rendering. (2006)
15. Hullin, M.B., Fuchs, M., Ihrke, I., Seidel, H.P., Lensch, H.P.A.: Fluorescent immersion range scanning. ACM Trans. on Graph. (ToG) **27** (2008) article no.87
16. Morris, N.J., Kutulakos, K.N.: Reconstructing the surface of inhomogeneous transparent scenes by scatter trace photography. In: Proc. of International Conference on Computer Vision (ICCV). (2007)
17. Narasimhan, S.G., Nayar, S.K., Sun, B., Koppal, S.J.: Structured light in scattering media. In: Proc. of International Conference on Computer Vision (ICCV). (2005)
18. Kim, J., Lanman, D., Mukaigawa, Y., Raskar, R.: Descattering transmission via angular filtering. In: Proc. of European Conference on Computer Vision (ECCV). (2010)
19. Treibitz, T., Schechner, Y.Y.: Instant 3descatter. In: Proc. of IEEE Conference on Computer Vision and Pattern Recognition (CVPR). (2006)
20. Florescu, L., Schotland, J.C., Markel, V.A.: Single-scattering optical tomography. Physical Review E **79** (2009) 036607
21. Mukaigawa, Y., Yagi, Y., Raskar, R.: Analysis of light transport in scattering media. In: Proc. of IEEE Conference on Computer Vision and Pattern Recognition (CVPR). (2010)
22. Narasimhan, S.G., Gupta, M., Donner, C., Ramamoorthi, R., Nayar, S.K., Jensen, H.W.: Acquiring scattering properties of participating media by dilution. In: Proc. ACM SIGGRAPH. (2006) 1003–1012
23. Hawkins, T., Einarsson, P., Debevec, P.: Acquisition of time-varying participating media. ACM Trans. on Graph. (ToG) **24** (2005) 812–815
24. Gu, J., Nayar, S.K., Grinspun, E.: Compressive structured light for recovering inhomogeneous participating media. In: Proc. of European Conference on Computer Vision (ECCV). (2008)
25. Nayar, S.K., Krishnan, G., Grossberg, M.D., Raskar, R.: Fast separation of direct and global components of a scene using high frequency illumination. Proc. ACM SIGGRAPH **25** (2006) 935–944
26. Nayar, S.K., Ikeuchi, K., Kanade, T.: Shape from interreflections. International Journal of Computer Vision (IJCV) **6** (1991) 173–195
27. Liu, S., Ng, T.T., Matsushita, Y.: Shape from second-bounce of light transport. In: Proc. of European Conference on Computer Vision (ECCV). (2010)
28. Beer, A.: Bestimmung der absorption des rothen lichts in farbigen flussigkeiten. Annalen der Physik und Chemie **86** (1852) 78–88
29. Henyey, L.G., Greenstein, J.L.: Diffuse radiation in the galaxy. Astrophysical Journal **93** (1941) 70–83
30. Kennedy, J., Eberhart, R.C.: Particle swarm optimization. In: IEEE International Conference on Neural Networks. (1995)
31. Nelder, J.A., Mead, R.: A simplex method for function minimization. The Computer Journal **7** (1965) 308–313